Deep–Sea Research I 193 (2023) 103952

Contents lists available at ScienceDirect

Deep-Sea Research Part I

journal homepage: www.elsevier.com/locate/dsri

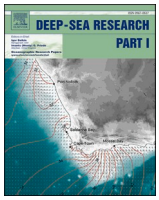

Contrasting phytoplankton composition and primary productivity in multiple mesoscale eddies along the East Australian coast

Giselle F. Firme [a,*], David J. Hughes [a], Leonardo Laiolo [b], Moninya Roughan [c], Iain M. Suthers [d,e], Martina A. Doblin [a,e]

[a] University of Technology Sydney, Climate Change Cluster, Ultimo, NSW, 2007, Australia
[b] Integrated Marine Observing System (IMOS), University of Tasmania, Private Bag 110, Hobart, Tas. 7001, Australia
[c] Regional and Coastal Oceanography Laboratory, School of Mathematics and Statistics, UNSW Australia, Sydney, Australia
[d] Evolution and Ecology Research Centre, School of Biological, Earth and Environmental Sciences, University of New South Wales, Kensington, NSW, 2052, Australia
[e] Sydney Institute of Marine Science, Mosman, NSW, 2088, Australia

ARTICLE INFO

Keywords:
Primary production
Climate change
Eddy
Carbon fixation
Cyclonic
EAC
Australia

ABSTRACT

Mesoscale eddies drive variability in phytoplankton functional trait composition and primary productivity (PP) relative to adjacent waters. Offshore waters in southeast Australia are subject to substantial mesoscale eddies that form when the East Australian Current (EAC) travels poleward along the coast, forming distinctive habitats in the upper ocean. Eddies provide an important enrichment mechanism in the nitrogen-limited waters of the Tasman Sea, yet there is limited knowledge of PP within cold- and warm-core eddies in the region and how physico-chemical and biological factors affect phytoplankton communities in this variable environment. We addressed the scarcity of observations by quantifying net PP using ^{13}C isotopic enrichment incubations of surface waters over 10 degrees of latitude, comparing phytoplankton species composition in five different environments: a coastal shelf station, an oceanic cold and warm-core eddy, and a coastal dipole. Cold-core (cyclonic) eddies were significantly more productive than their warm-core (anticyclonic) counterparts (~35 versus 0 mg C m^{-3} d^{-1}), with centric diatoms the most prominent phytoplankton group, with a relatively high centric:pennate ratio. The diffuse attenuation coefficient, K_d (PAR), and silicate were the best overall predictors of phytoplankton composition, explaining 88% of variation based on pigment analysis and size fractionation. Variance in net PP did not correlate significantly with physico-chemical parameters frequently used in PP models (temperature, K_d [PAR], Chl *a*), yet inclusion of size-fractionated Chl *a* generated substantial improvement in our statistical model (from 36 to 77%). We show that cold-core eddies play a key role in regulating PP in eastern Australian waters and highlight a need for eddy-resolving models to incorporate descriptors of phytoplankton size structure to improve the accuracy of PP forecasts in eddy intensive regions.

1. Introduction

Phytoplankton primary productivity (PP) regulates the global carbon cycle, underpins marine foodwebs and ultimately defines the carrying capacity of marine ecosystems (Behrenfeld and Falkowski, 1997). Phytoplankton biomass is however inherently patchy over space and time (Mahadevan and Campbell, 2002), and therefore development of tools to accurately model PP in the global ocean is a high priority for oceanographers (Martin et al., 2002).

Most ecosystem models of PP are based on satellite-retrieved data (notably Chlorophyll *a* [Chl *a*], solar irradiance and sea surface temperature [SST]), often calibrated against (simulated) in-situ measurements of carbon-incorporation (e.g. ^{13}C- and ^{14}C incubations) (Behrenfeld and Falkowski, 1997; Westberry et al., 2008; Dufois et al., 2017; Dutkiewicz et al., 2019). This approach has allowed oceanographers to establish empirical relationships between prevailing environmental conditions and PP rates, yet satellite-based models often contain significant uncertainty (Friedrichs et al., 2009; Milutinović and Bertino, 2011). While this is largely explained by the scarcity of in situ productivity measurements to validate and calibrate phytoplankton PP models, the presence of dynamic mesoscale ocean features - such as eddies – also contributes to regional PP variability.

* Corresponding author.
E-mail address: Giselle.Firme@student.uts.edu.au (G.F. Firme).

https://doi.org/10.1016/j.dsr.2022.103952
Received 20 June 2022; Received in revised form 6 December 2022; Accepted 13 December 2022
Available online 14 December 2022

Depending on their rotational direction and speed, mesoscale eddies can strongly influence the composition and productivity of entrained phytoplankton assemblages compared to surrounding oceanic waters. Cold-core (cyclonic/clockwise-turning in the southern hemisphere) eddies promote vertical advection of nutrients into the euphotic zone, stimulating phytoplankton photosynthesis and growth, and favour proliferation of larger phytoplankton taxa (McGillicuddy, 2016). In contrast, warm-core (anticyclonic/anticlockwise-turning in the southern hemisphere) eddies supress nutrient uplift, limit phytoplankton photosynthetic rates and ultimately favour small phytoplankton (Baird et al., 2011). Importantly, the rotational speed of eddies decreases with time – and thus environmental gradients between eddies and the surrounding water weaken with increasing eddy age. Mesoscale eddies (up to 500 km wide) can persist for up to two years (Chelton et al., 2011; Jeffrey and Hallegraeff, 1980) and can significantly influence phytoplankton productivity in oligotrophic regions (Baltar et al., 2010; Chelton et al., 2011), with cold-core eddies enhancing global oceanic PP by an estimated 20% (Falkowski et al., 1991). Invariably, deviations occur due to the dynamic and fluid nature of mesoscale processes, where mixed-layer instability can produce heterogeneity of nutrient or light availability, or subduction of viable cells, possibly altering expected PP responses within an eddy (Mahadevan, 2016).

Understanding the influence of mesoscale eddies on PP variability is particularly important for regions influenced by western boundary currents, where hydrodynamic conditions favour prolific eddy formation (Kamenkovich et al., 1986). The East Australian Current (EAC) is the western boundary current of the South Pacific gyre, noted for its mesoscale variability that exhibits a strong seasonal cycle (Malan et al., 2020; Ridgway, 1997; Schaeffer et al., 2017). The EAC transports warm, oligotrophic water from the Coral Sea poleward along the edge of the continental shelf until it separates from the coast, at ~31–32°S, shedding large warm-core eddies (Cetina-Heredia et al., 2014). These eddies flow eastward towards New Zealand, forming the EAC eastern extension. The remaining half of the EAC forms the southern extension (Oke et al., 2019) breaking into a substantial and complex eddy field south of the separation zone, known as "Eddy Avenue," with over 1.5 cyclonic eddies observed on any given day (Everett et al., 2012). Associated with the EAC separation are both large and small cold-core eddies. Small frontal eddies form on the inside edge of the EAC jet (Roughan et al., 2017; Schaeffer et al., 2017) and tend to propagate poleward (Cetina--Heredia et al., 2019) at times as eddy dipole pairs (Malan et al., 2020), whereas large eddies are formed in the Tasman Sea and propagate westward, intersecting with the EAC jet (Malan et al., 2020).

In recent years, both the strength and frequency of eddies, and eddy-driven transport, have increased in this region due to climate change-driven strengthening of the EAC (Cetina-Heredia et al., 2014; Matear et al., 2013). Understanding how changing eddy dynamics may impact future PP in this region is particularly important because despite being an area of relatively low productivity and carbon export (Doblin et al., 2016), it paradoxically supports a valuable longline fishing industry (McIlgorm et al., 2010).

Presently, our understanding of the factors regulating phytoplankton PP within cold vs warm-core eddies, and how they vary over time is incomplete. Only a handful of studies have examined in situ PP associated with the EAC, where measurements have been limited; i.e., capturing one to two eddies per voyage and possibly confounding variability between types of eddies, with eddies of different age and source water (Doblin et al., 2016; Everett and Doblin, 2015; Hassler et al., 2011).

In this study we utilise ^{13}C bottle incubations to quantify phytoplankton PP in multiple eddies (both cold and warm-core) along the EAC, including a dipole eddy pair of the same age. We assess both phytoplankton community structure and prevailing physico-chemical conditions in order to better understand the environmental factors associated with PP variability in contrasting eddy types.

2. Materials and methods

2.1. Study area and sample collection

Hydrographic and biological measurements were performed in southeastern Australia between August 31st to September 18th, 2017, aboard the *RV Investigator* (voyage: INV2017_v04). This voyage was part of a larger effort to quantify the physical oceanography and pelagic ecosystem of eddies in the region, examining organisms from microbes to mammals (Archer et al., 2020; Malan et al., 2020). The sampling area extended 10 degrees of latitude, from offshore of Brisbane, QLD (27.3°S) to south of Montague Island, NSW (35.6°S; Fig. 1). Two eddies were sampled north of the Tasman Front: a ~150 km diameter cold-core eddy off the coast of Brisbane (~27.5° S; "ACC"), and a ~200 km diameter warm-core eddy, formed from the retroflection of the EAC (~33° S; "WC"). An eddy dipole was sampled south of the Tasman Front (~35° S), including a cold-core ("DCC") and warm-core ("DWC") eddy that were both ~100 km in diameter (Archer et al., 2020). The voyage plan also permitted us to sample a coastal reference station outside of the eddy field (adjacent to Newcastle NSW, ~33° S; "C"), although unfortunately it did not provide an opportunity to also sample an oceanic (i.e. oligotrophic) reference station - which would arguably have provided additional insight into the regional impact of the eddy field.

Voyage sampling designs necessarily trade off sampling resolution in one eddy with sampling many eddies, so in order to increase our understanding of spatial variability of PP, we sampled ten stations within a two-week window, enabling us to minimise variance caused by season and increase our ability to compare PP in different eddy types.

2.2. Physico-chemical variables

During the voyage, there were 38 stations sampled in the wider study (Kwong et al., 2020; Malan et al., 2020), where Conductivity Temperature and Depth (CTD; SBE911, Seabird Electronics, USA) profiles to 1000 m depth were collected, with the vertical distribution of phytoplankton assessed using a calibrated Aquatracker Mk3 fluorometer (Chelsea Technology Group, London, UK). At 10 of these stations, water for PP incubations was collected (see Fig. 1 for CTD stations corresponding to PP measurements). Mixed layer depth (MLD) was calculated from each CTD profile using the threshold method, applying a MLD definition of $\Delta T = 0.5$ °C (Kara et al., 2000). The coastal station was the exception, being in only 146 m of water, where the entire water column was considered the MLD. Seawater samples were collected by 12 L Niskin bottles housed in a 36-bottle rosette sampler, triggered electronically at depths of 1000 m, 500 m, 300 m, 200 m, 100 m, 80 m, 50m, 20 m and surface (5–10 m) during upcasts. Dissolved oxygen concentrations were determined using the Winkler-titration method (Strickland and Parsons, 1972). Samples from all stations were immediately analysed at sea for dissolved inorganic nutrient concentrations, specifically: nitrate plus nitrite (NO_x), ammonium (NH_4^+), phosphate (PO_4^{3-}) and silicate (Si) using automated continuous flow with colorimetric detection following the protocol of Rees et al. (2019). A photosynthetic active radiation (PAR) sensor (Biospherical Instruments Inc., San Diego, USA) was installed on the auxiliary, analog-to-digital channel of the CTD, and data collected was subsequently processed within the CSIRO Oceans and Atmosphere Information and Data Centre in Hobart. The diffuse attenuation coefficient of PAR (K_d [PAR]) for each PP station was calculated according to Eq. (1):

$$Kd(z) = \frac{\ln E_{d0} - \ln E_{dz}}{Z} \quad (1)$$

where E_{dz} is the downwelling irradiance at depth Z, E_{d0} is the downwelling irradiance just below the surface, and K_d is the attenuation coefficient (Morris, 2009). In this case, we calculated Z as 1% attenuation depth, and used PAR measured at solar noon to estimate K_d (PAR) in

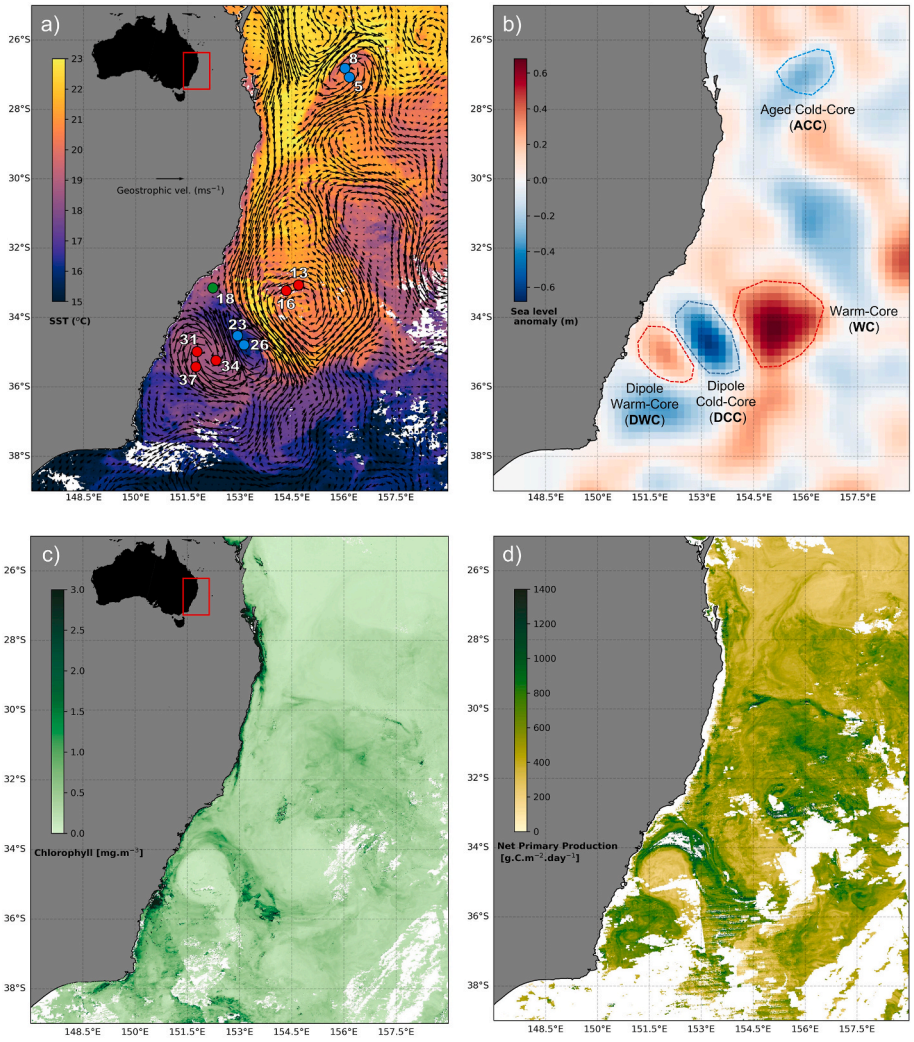

Fig. 1a. Satellite image of sea surface temperature (SST) and geostrophic velocity off southeast Australia, overlaid with conductivity temperature and depth (CTD) stations sampling locations for cold-core (blue circles) and warm-core (red circles) eddies, and the coastal station (green circle). **1b.** Satellite image of sea level anomaly overlaid with distinct water masses sampled: aged cold-core eddy (ACC), warm-core eddy (WC) and dipole cold- and warm-core pair (DCC and DWC). SST image sourced from the Integrated Marine Observing System (IMOS) (http://imos.aodn.org.au). Geostrophic velocities are shown as black arrows, with length indicating both speed and distance travelled by surface water over the previous 24 h.**1c**. Satellite image of surface Chlorophyll *a* using the OC3 algorithm (mg m^{-3}) **1d**. Net Primary Productivity estimated using the GSM model and Eppley-VGPM algorithm (g.C.m^{-2}. d^{-1}). Both images are 8-day composite sourced from IMOS - SRS - MODIS - 01 day. Data sourced from the Australian Ocean Data Network (AODN) (https://portal.aodn.org.au/).

order to minimise incident light angle variability.

2.3. Size-fractionated chlorophyll a

Size-fractionated Chl *a* was determined based on the method of Arar and Collins (1997). Triplicate seawater samples were filtered onto 10 μm polycarbonate (Merck Millipore, USA), 2.0 μm and 0.3 μm glass fibre filters (Advantec, Japan). After filtering 0.5–1 L of seawater (depending on biomass present), filters were stored at −80 °C for later analysis. Filters were subsequently thawed to room temperature, and pigments were extracted in 90% acetone at 4 °C in darkness for 24 h as per Hughes et al. (2020), and Chl *a* content was determined fluorometrically using a benchtop fluorometer (Trilogy, Turner Designs, California, USA), fitted with a Chl *a* Acidification Module and pre-calibrated against a pure Chl *a* standard (Sigma-Aldrich Pty Ltd, Castle Hill, Australia).

2.4. Phytoplankton pigment analysis (HPLC)

Phytoplankton pigment composition reflects both the underlying taxonomic composition and the photo-physiological status of the phytoplankton assemblage, both linked to environmental variables such as light and nutrient availability (Claustre et al., 1994). To provide a snapshot of the representative phytoplankton assemblage in each eddy environment and limit variation due to diel acclimation, we opted to perform additional casts at the same location at solar noon after first verifying that the same parcel of water was being sampled (by assessing salinity, temperature and MLD profiles).

Triplicate samples for pigments were filtered onto 0.7 μm glass fibre filters (GF/F Whatman, USA). Sample volumes filtered were variable but ranged from 0.5 to 1 L. Samples were stored in liquid nitrogen and analysed onshore by high performance liquid chromatography (HPLC). Biomarker pigments were used to infer the distribution of dominant algal classes and functional groups as per Thompson et al. (2011). Each biomarker pigment was normalised against total Chl *a* (i.e., the sum of Monovinyl and Divinyl Chl *a*) to account for variation in phytoplankton biomass per sample. Briefly, biomarker pigments represent the following phytoplankton classes: autotrophic dinoflagellates (Peridinin), pelagophytes (19-But-fucoxanthin), diatoms (Fucoxanthin-although also found in prymnesiophytes, chrysophytes, pelagophytes and raphidophytes), chlorophytes (Neoxanthin, Violaxanthin + Chl *b*), prasinophytes (Prasinoxanthin), coccolithophorids (19- Hex-fucoxanthin), *Synechococcus* (Zeaxanthin), cryptophytes (Alloxanthin), and *Prochlorococcus* (Divinyl Chl *a*). Pigment biomarker and quality control were performed as per (Thompson et al., 2011) and photosynthetic (PSC) and photo-protective (PPC) pigment contributions were calculated as per Barlow et al. (2007). Pigments were also used to determine the Shannon-Weiner Diversity Index (H'), to compare phytoplankton diversity in the different water masses sampled (Noble et al., 2003).

2.5. Phytoplankton identification

Seawater samples for micro-phytoplankton analysis (cold-core CTD

stations ACC 8, DCC 23, warm-core stations WC 13, DWC 31 and the coastal reference station C18; Fig. 1) were fixed with 1% Lugol's solution and stored in tinted glass bottles for later taxonomic analysis. The 1 L sample was concentrated by settling for 48 h in a 1 L glass measuring cylinder, after which 900 mL of the supernatant was carefully siphoned off from the top using a glass Pasteur pipette under gentle vacuum. The remaining 100 mL was allowed to settle for a further 48 h in a 100 mL glass measuring cylinder, after which 90 mL supernatant was removed. The remaining 10 mL was kept refrigerated (4 °C) in a dark glass vial until subsequent phytoplankton identification and enumeration. From this 10 mL concentrated sample, 1 mL was loaded into a glass Sedgwick-Rafter counting chamber and enumerated on a compound microscope (Nikon Eclipse Ci-L, Nikon Instruments, Japan). A minimum of 200 cells were counted per sample at 400x magnification, and phytoplankton cells >10 μm diameter were identified down to the lowest taxonomic level possible (to genus level in most cases).

2.6. Primary productivity (^{13}C-incubations)

Surface water (5–10 m depth) was collected at dawn and stored in an acid-washed dark container prior to 13^C incubation assays. To estimate the size-fractionated particulate organic carbon (POC) of the phytoplankton community, triplicate water samples were passed through 200 μm mesh to remove zooplankton grazers and 2 L was then immediately filtered onto pre-combusted (450 °C for 4 h) 2.0 μm nominal pore size 25 mm diameter glass fibre filters (GF/F, Advantec) to capture the >2.0 μm size fraction. A further set of triplicate, 2 L samples were filtered in sequence onto 25 mm filters as follows: 10 μm polycarbonate membrane filter (Merck Millipore, USA), 2.0 μm and 0.3 μm nominal pore size filters (GF/F, Advantec). Polycarbonate filters were discarded, and glass fibre filters were wrapped in aluminium foil and placed in a −80 °C freezer for storage and later analysis. The POC of the >10 μm phytoplankton cell size class was estimated by the mathematical difference between the >2.0 μm size fraction filtered alone and the 2.0 μm–10 μm size fraction captured sequentially with the 10 μm polycarbonate membrane filter and 2.0 μm glass fibre filter.

The remaining water was used to fill triplicate 4 L, acid–washed, polycarbonate bottles (Nalgene, ThermoFisher, USA) as previously described. Each bottle was enriched with 10 μL $NaH^{13}CO_3$ to a final concentration of 5 mM, gently mixed and placed into flow-through deckboard incubators, at 40% of incident light using a blue filter (#172 Lagoon Blue, Lee Filters, Andover, UK) to modify spectral transmission and approximate in situ conditions as per Hughes et al. (2018b). Bottles were incubated at ambient sea-surface temperatures for 24 h – i.e. a complete diel cycle to measure net PP (see Regaudie-de-Gioux et al., 2014), after which samples were filtered onto pre-combusted filters and frozen as described above for subsequent carbon isotope analysis. Filters were dried at 60 °C for 24 h and carbon isotope analysis was performed at the Isotope Laboratory, University of Hawaii. Net PP rates were calculated based on (Hama et al., 1983) according to Eq. (2):

$$P = \frac{\Delta C}{t} = \frac{C * (a_{is} - a_{ns})}{t * (a_{ic} - a_{ns})} \quad (2)$$

where P is the photosynthetic rate (mg C L^{-1} h^{-1}), ΔC is the increase in POC during the incubation (mg C L^{-1}), t is the duration of incubation in hours, C is POC in the incubated sample at the end of incubation (mg C L^{-1}), a_{is} is the atom % of ^{13}C in the incubated sample, a_{ns} is the atom % of ^{13}C in the natural sample, and a_{ic} is the atom % of ^{13}C in the total inorganic carbon. In the rare event that calculations produced negative PP values (which occurred at two stations in the dipole warm-core eddy, #34 and #37, See Fig. 1), such values were presumed to reflect low signal-to-noise in the ^{13}C measurements, and were left uncorrected.

2.7. Treatment of data and statistical analysis

Analysis of variance (ANOVA) was performed to evaluate statistical differences in total Chl *a* and net PP between eddies. Prior to ANOVA, data residuals were tested for normality of distribution and homogeneity of variance using Shapiro-Wilk's and Levene's tests respectively. ANOVAs were performed using SPSS v20.0 software (SPSS Inc, Chicago, IL, USA). Nonmetric multidimensional scaling (nMDS) was used to visualise patterns in physico-chemical variables (PRIMER v.6.0 software, PRIMER-E, Plymouth, UK). Hierarchical cluster analysis (HCA) with a SIMPROF test ($p = 0.05$) was performed on a Euclidean resemblance matrix of square-root transformed physico-chemical variables (K_d [PAR], MLD, temperature, salinity, NH_4^+, NO_x, PO_4^{3-} and Si) to identify stations of similar hydrography. Student's *t*-tests were used to test for differences between station clusters identified by HCA for variables after first verifying assumptions of normality and equal variance (tested for by Kolmogorov-Smirnov and Levene's tests, respectively), using Sigmaplot v11.0 (Systat Software Inc., California, USA). Where one or both assumptions were not met, differences between clusters were instead assessed using the non-parametric Mann-Whitney Rank Sum test (Sigmaplot v11.0, Systat Software Inc.).

2.8. Predicting biological responses of eddies from environmental variables

Previous studies have established a relationship between cold-core eddies and high phytoplankton biomass (usually comprising large-sized phytoplankton taxa such as diatoms), with upwelling leading to higher rates of nutrient delivery to euphotic waters, and therefore enhanced productivity (Laiolo et al., 2018; Mahadevan, 2016; Roughan et al., 2017). In contrast, warm-core eddies are commonly dominated by smaller phytoplankton cells typical of oligotrophic water masses, and are generally less productive due to stratification of the water column which limits nutrient uplift (Oke and Griffin, 2011; Suthers et al., 2011). Given the notable differences in biotic and abiotic characteristics between cold- and warm-core eddies, we investigated whether the biological status of the phytoplankton community could be predicted solely from knowledge of prevailing physico-chemical conditions.

Distance-based linear modelling/regression (DistLM) was performed within Primer-e (PRIMER v.6.0 software, PRIMER-E, Plymouth, UK) to examine the extent to which variation in Chl *a* biomass and phytoplankton composition (HPLC) could be explained by core environmental variables (specifically: K_d [PAR], MLD, temperature, salinity and nutrients). Similarly, we examined how much variation in PP was correlated with both environmental and biological variables (specifically: total Chl *a*, size-fractionated Chl *a*, Chl *a* normalised pigments, pigment indices, and phytoplankton diversity, H').

Prior to DistLM analysis, the distribution of each physico-chemical variable was assessed using draftsman's plots and correlated co-variables were identified from Pearson's correlation matrices. Variables with skewed distribution were log transformed, and if pairs of variables had a Pearson's correlation co-efficient of >0.9, one of the pair was excluded from subsequent analyses (e.g., PO_4^{3-} and NO_x were excluded as they were both strongly correlated with Si).

To understand the respective predictive power of the measured variables, we initially performed DistLM analysis selecting only environmental (physico-chemical) variables as available predictor variables. For PP, we again excluded co-correlations (fucoxanthin, Dia_{DP}, total Chl *a*, and salinity were excluded as they correlated with 10 μm Chl *a*) and then performed the analysis for biological variables, and finally selected the variables based on the most statistical explanatory power revealed in the marginal tests, relevant for both physico-chemical and biological predictors. To obtain the most parsimonious model at each step, we used the "best" model selection routine based on 9999 permutations with Akaike information criterion (AICc - corrected for small sample number), which incorporates a penalty factor for increasing the number of

predictor variables (Anderson et al., 2008).

To examine whether satellite data alone could explain variance in eddy PP, we selected a specific set of predictor variables representing proxies for remotely-sensed data (i.e. temperature, K_d [PAR] and Chl *a*) by selecting "specified solutions" in the DistLM model. We next included biological variables that are routinely collected on research voyages (size-fractionated Chl *a*) and are inexpensive to examine, to determine if this improved model performance. Distance-based redundancy analysis (dbRDA) plots were generated to enable two-dimensional visualisation of the best DistLM models.

3. Results

Four eddies with different physico-chemical characteristics were sampled in southeastern Australian waters during August–September 2017 (Fig. 1). The northern cold-core eddy (aged cold-core, ACC) off the coast of Brisbane (~27° S) had surface temperatures that were 2–4 °C cooler than surrounding waters (Fig. 1a). This was an older eddy that had formed in the Coral Sea nearly three months earlier (approximately mid-July), travelled coastward and dissipated by the end of September shortly after our voyage. Further south, we encountered a large warm-core eddy shed a few weeks earlier from the EAC jet in August, with surface temperatures of 19–21 °C. The final eddies sampled consisted of a cold-core and warm-core eddy dipole, formed in early August, south of the Tasman front around 32° S (Fig. 1a). The dipole was most active (i.e., exhibiting strongest SST and velocity gradients) in early September (Malan et al., 2020), coinciding with our sampling. The temperature gradient across the eddy dipole was 3–4 °C, with temperatures of 19 °C in the core of the dipole warm-core and 16 °C in the core of the dipole cold-core (Fig. 1a). By the end of September, the dipole had dissipated (see Archer et al., 2020, their Fig. 2 for evolution of the eddy dipole pair). The warm-core dipole had a physico-chemical signature similar to the coastal reference station, with a surface temperature of 18 °C suggesting entrainment of coastal waters (Fig. 2a and b). In summary, the large warm-core eddy sampled was of similar age to the eddy dipole, and formed an age contrast with the ~3 month old cold core eddy sampled in the northern part of the study domain. Although our study examined surface waters only, the stations sampled were vertically well-mixed and no subsurface chlorophyll maxima were found. Satellite algorithms use surface Chl *a* data and infer depth distribution of PP (Fig. 1c and d), therefore it is important to validate surface PP values, as we have done in this study.

3.1. Physico-chemical characteristics

Both warm-core eddies had similar water mass vertical profiles (Fig. 2a). Specifically, they exhibited deeper mixed layers (~300 m) and weaker ΔT (the difference in temperature between the surface and thermocline lower limits) than both cold-core eddies, with surface temperatures ranging from 19.9 °C (WC 13) to 18.5 °C (DWC 34) (Fig. 1, Table 1). Surface salinity at both these warm-core eddy locations was ~35.7 PSU (Fig. 2a, Table 1), and surface nutrient concentrations ranged from 1.23 to 2.31 μM NO_x, 0.14–0.24 μM $PO_4^{-3}$and 0.66–0.96 μM Si, with higher values at the dipole stations relative to the northern stations. Dissolved oxygen in surface waters ranged from 214.12 μM (WC 13) to 218.90 μM (DWC 31). The lowest K_d (PAR) was found in the dipole warm-core (0.04 m^{-1}), whereas the warm-core eddy had intermediate values (0.06–0.64 m^{-1}) (Table 1).

In contrast, both cold-core eddies had shallower mixed layer depths (76 m for the aged cold-core, and 100 m for the dipole cold-core eddy), and stronger ΔT, with surface temperatures ranging from 15.9 °C (DCC 23) to 19.9 °C (ACC 5) (Fig. 2a). The dipole cold-core eddy had the highest surface concentration of nutrients: 3.02–3.44 μM NO_x, 0.32–0.34 μM PO_4^{-3} and 0.98–1.18 μM Si, however surface NO_x concentration in the aged cold-core eddy had been drawn down to the lowest values observed during the voyage (0.13–0.31 μM), whereas NH_4^+

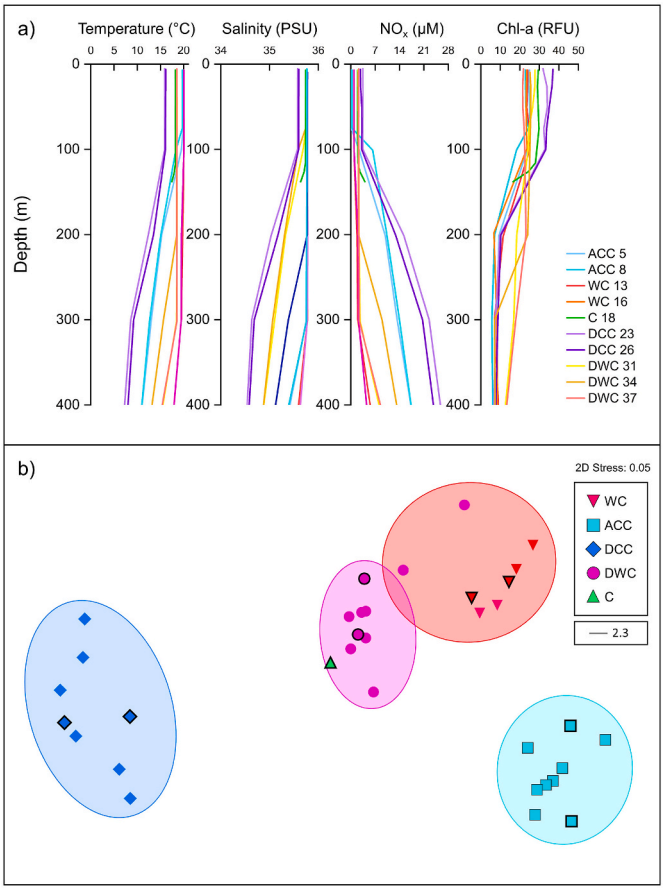

Fig. 2. a. Temperature, salinity, nitrate + nitrite (NO_x) and Chlorophyll *a* depth profiles of aged cold-core (ACC 5, 8), warm-core (WC 13, 16), the dipole cold- and warm-core eddies (DCC 23, 26, and DWC 31, 34 and 37), and coastal station (C18). **b.** Nonmetric Multidimensional Scaling (nMDS) ordination plot with overlaid SIMPROF clusters (identified by solid-coloured lines) visualizing the grouping of all 38 hydrographic stations sampled according to physio-chemical characteristics (mixed layer depth, temperature, salinity, dissolved oxygen, K_d [PAR], phosphate [PO_4^{-3}], silicate [Si], nitrate and nitrite [NO_x]). The specific stations corresponding to PP measurements performed are indicated by symbols with a thick bold border.

was at a maximum (0.14–0.23 μM) (Table 1). Surface PO_4^{-3} and Si values in the aged cold-core eddy were also found to be the lowest of all stations sampled: 0.14 μM and 0.50 μM respectively. Surface dissolved oxygen concentrations were higher in the cold-core eddies ranging from 219.88 μM (ACC 8) to 237.69 μM (DCC 26). The greatest light attenuation was found in the dipole cold-core eddy (0.089 m^{-1}) with lower values of K_d (PAR) found in the aged cold-core eddy (0.056–0.066 m^{-1}).

The coastal station (C18) was situated over the continental shelf and only 146 m in depth, however temperature, salinity, and nutrients were similar to the dipole warm-core average values, while dissolved oxygen and K_d (PAR) values were slightly higher (Table 1).

When considering all the physico-chemical variables, the four eddies had distinct surface water mass properties, with the aged cold-core eddy stations more closely resembling the characteristics of warm-core eddies as shown by their clustering in ordinate space (Fig. 2b). Broadly, eddy types could be grouped according to physico-chemical properties.

3.2. Phytoplankton biomass, size structure and composition

Total Chl *a* at the surface ranged from 0.22 to 1.28 μg L^{-1} over the study area, with the lowest values measured in the dipole warm-core eddy (DWC 37) and the highest values in its cold-core counterpart (DCC 26, Table 2). Average Chl *a* concentration was higher in the dipole

Table 1
Summary of physico-chemical properties for surface water (5–10m): Temperature (°C), Salinity (PSU), Mixed Layer Depth (MLD, m), Nitrate plus nitrite (NO_x, μM), Phosphate (PO_4^{-3}, μM), Silicate (Si, μM), Ammonia (NH_4^+, μM), Oxygen (O_2, μM), and the diffuse attenuation coefficient of photosynthetically active radiation (Kd [PAR]). Average values ± standard error ($n = 3$) or range ($n = 2$) for water masses sampled from 2–16 September 2017, where n is the number of Conductivity, Temperature and Depth (CTD) casts where primary productivity (PP) measurements were performed in each water mass: aged cold-core (ACC), warm-core (WC), dipole cold-core (DCC) and warm-core (DWC) eddies, and coastal reference station.

Water	n	Temp	Salinity	MLD	NO_x	PO_4^{-3}	Si	NH_4^+	O_2	K_d (PAR)
ACC	2	19.73–19.87	35.74–35.75	75.5–76.0	0.13–0.32	0.14	0.50	0.14–0.23	219.88–230.37	0.056–0.062
WC	2	19.96–19.97	35.76	300.3–301.5	1.23–1.26	0.18	0.66–0.67	0.02–0.05	214.12–214.16	0.055–0.064
DCC	2	15.91–16.11	35.57–35.59	99.7–100.2	3.02–3.44	0.32–0.34	0.98–1.18	0.0–0.02	236.75–237.69	0.082–0.094
DWC	3	18.50 (0.02)	35.77 (0.00)	251 (34)	2.23 (0.04)	0.24 (0.00)	0.94 (0.02)	0.00 (0.00)	221.30 (4.06)	0.040 (0.00)
Coastal	1	18.20	35.73	146	2.11	0.23	0.96	0.03	222.18	0.067

Table 2
Biological properties in surface water (5–10m depth) for water masses: total Chlorophyll *a* (Chl *a*, μg L^{-1}), net primary productivity PP, (mg C m^{-3} d^{-1}), phytoplankton cell abundance data determined by cell counts (Cell abundance, 10^6 cells L^{-1}), Shannon-Wiener Diversity Index (H′) as determined using high performance liquid chromatography (HPLC) data, centric to pennate diatom ratio (Centric:Pennate), percentage of phytoplankton cells of sizes equal or larger than 10 μm (cells ≥10 μm, %), and percentage of phytoplankton cells of sizes smaller than 10 μm (cells <10 μm, %) determined by cell counts at each water mass. Total Chl *a*, NPP and H': aged cold-core (ACC) $n = 2$, warm-core (WC) $n = 2$, dipole cold-core (DCC) $n = 2$ dipole warm-core (DWC) $n = 3$, coastal reference (C), $n = 1$; except for DCC where PP was performed only once in this water mass.

Water	Total Chl *a* ugL^{-1}	PP mg C m^{-3} d^{-1}	Cell abundance 10^6cellsL^{-1}	H′	Centric:Pennate	% cells ≥10 μm	% cells <10 μm
ACC	0.40 ± 0.22	16.68 ± 6.62	21.10	1.91 ± 0.01	3.64	53.27	46.73
WC	0.30 ± 0.00	3.84 ± 4.41	28.93	1.92 ± 0.00	0.10	27.42	72.58
DCC	1.15 ± 0.17	35.76	73.39	1.60 ± 0.04	1.94	60.98	39.02
DWC	0.33 ± 0.11	−0.04 ± 8.92	24.60	1.67 ± 0.08	0.37	35.77	64.23
C	0.55 ± 0.02	7.45	99.38	1.88	2.04	9.75	89.66

cold-core eddy compared to the other eddies (ANOVA, $F_{2,6} = 0.002$, $P < 0.05$, Bonferroni post-hoc test), yet there was no difference in total Chl *a* between the remaining eddies (aged cold-core, warm-core and dipole warm-core). When the coastal station was included no significant difference between stations was found ($P > 0.05$).

The dipole cold-core eddy was dominated by larger-sized phytoplankton (>10 μm), which comprised 63–83% of total Chl *a*. In contrast, phytoplankton assemblages in warm-core eddies were dominated by the smallest phytoplankton size class (0.3–2 μm), which accounted for over half of total Chl *a* in both the dipole warm-core and warm-core eddies (54 and 56%, respectively). The phytoplankton size fraction within the aged cold-core eddy was mainly split between the 0.3–2 μm and 2–10 μm size classes, comprising 96% of the total Chl *a* (0.25–0.56 μg L^{-1}). In the coastal station only 17% of the phytoplankton assemblage was larger than 10 μm (Fig. 3a).

The dipole cold-core stations were dominated by diatoms (comprising approximately 60% of total Chl *a*), while stations in both warm-core and aged cold-core eddies showed a more diverse phytoplankton assemblage comprising fewer diatoms (8–13%, aged cold-core; 9–11% warm-core and dipole warm-core), with coccolithophorids (37–50%) and pelagophytes (21–40%) instead comprising the bulk of the taxa present (Fig. 3b). Pigment derived estimates of *Prochlorococcus* were highest in both northernmost eddies (aged cold-core and warm-core) comprising 5–12%.

Phytoplankton cells ≥10 μm diameter numerically dominated cold-core stations (~53–60% of total cells), while cells <10 μm diameter prevailed in the warm-core stations (~64–72% of total cells) and the coastal station (~89% of total cells), with a reduced total abundance in the aged cold-core and warm-core stations, in comparison to the dipole cold-core station and the coastal station (Table 2). Centric diatoms were more numerous than pennate diatoms in the cold-core and coastal stations, while pennates were more abundant in the warm-core eddies and the aged cold core eddy, with the centric: pennate ratio ranging from 0.1 (WC 13) to 3.6 (ACC 8) (Table 2). In the dipole cold-core eddy 39% of the diatoms were larger than 20 μm in contrast to 25% of the aged cold-core eddy and 5% of the coastal station (Supplementary Table S2).

The photoprotective to photosynthetic pigment ratio (PPC:PSC) ranged from 0.07 to 0.21, averaging 0.13 across all eddy types, however

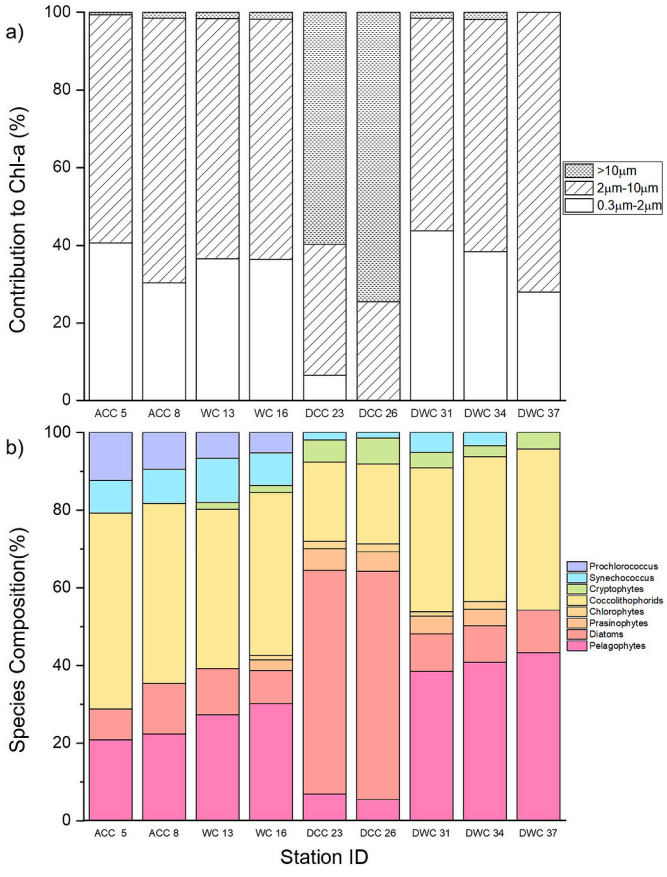

Fig. 3. a. Phytoplankton size class fractions reflected as percentage contribution to total Chlorophyll *a* (Chl *a*) for aged cold-core (ACC), warm-core (WC), coastal (C), dipole cold-core (DCC) and dipole warm-core (DWC) eddies and **b.** Phytoplankton species composition – reflected as percentage distribution of dominant algal classes normalised by total Chl *a* based on high performance liquid chromatography (HPLC) analysis of pigments.

there was no difference between aged cold-core, warm-core and the dipole cold-core eddies, nor when stations were grouped between warm-core and cold-core eddies ($P > 0.05$, Kruskall-Wallis) (Supplementary Table S1). Lutein and diatoxanthin are photoprotective carotenoids that were not included in the HPLC analysis and are two of the five components of PPC, therefore it is possible that values reported are underestimates. The largest photosynthetic carotenoid (PSC) values were found in the dipole cold-core eddy (0.75) and the lowest in the dipole warm-core eddy (0.14) (data not shown). The particulate organic carbon to nitrogen ratio ranged from 7.42 to 16.17, with an average of 11.18, however again, no significant difference between eddy types was found ($P > 0.05$, T-test) (Supplementary Fig. S1).

3.3. Primary productivity

Total PP, as well as PP of the >10 μm size class was greater in cold-core eddies (ANOVA, $F_{1,7} = 10.94$, $P < 0.05$ and $F_{1,7} = 9.82$, $P < 0.05$ respectively). Total PP ranged from 12 mg C m^{-3} d^{-1} in the aged cold-core eddy to 35.7 mg C m^{-3} d^{-1} in the dipole cold core eddy, whereas highest productivity in the warm-core eddies reached only 9.8 mg C m^{-3} d^{-1} (Fig. 4). There were significant differences in net PP of the total phytoplankton community and the larger size class between water masses (ANOVA $F_{2,7} = 11.41$, $P < 0.05$, and $F_{2,7} = 10.87$, $P < 0.05$ respectively), however it was not possible to identify specific differences via a post-hoc analysis due to the low sample size.

3.4. Predicting biological responses of eddies from physico-chemical variables

Distance based linear regression showed that salinity, and K_d (PAR), were significantly correlated ($P < 0.01$) to the variance in biomass and composition of phytoplankton. Salinity alone was associated with ~70% of variation in phytoplankton composition, whereas K_d (PAR) and Si were the overall best predictors explaining 88% of the phytoplankton composition based on HPLC pigment analysis and Chl *a* size fractionation (Table 3, Supplementary Fig. S2). Including salinity improved the statistical model to 92%.

3.5. Predicting primary productivity from physico-chemical and biological variables

Principal coordinate analysis (PCO) of the physico-chemical and biological variables revealed grouping of stations into four distinct water masses, where the percentage of total variation inherent in the resemblance matrix was 80%, showing a clear separation of stations among all four eddies (Supplementary Fig. S3). None of the physico-chemical variables were significant predictors for PP in the distinct water masses, although when combined, K_d (PAR), temperature and Si explained up to 47% of PP variation in the dataset. In contrast, changes in biological variables featured the presence of prokaryotes ($P < 0.05$, $R^2 = 0.464$), the ratio of photoprotective to photosynthetic pigments, PPC:PSC ($P < 0.05$, $R^2 = 0.399$) and the Shannon-Weiner Diversity Index, H′, ($P < 0.05$, $R^2 = 0.377$) as significant predictor variables for PP. Additionally, when H′, prokaryotes and large phytoplankton were included, the statistical model improved to 74% (Table 4). The combination of physico-chemical and biological variables resulted in PPC:PSC and H′ being significant predictors of PP ($P < 0.05$), however the modelling process selected H', temperature and Si as overall best predictors, explaining ~ 70% of variability in PP (Table 4).

When specifying variables that are routinely included in PP modelling, and easily obtained utilising satellites (i.e., temperature, K_d [PAR] and Chl *a*), only 36% of variability in PP was explained. When routinely collected, cost-effective in situ parameters were included in the DistLM model, namely size fractionated Chl *a*, the predictive power of the model improved to explain 77% of variability in PP (Table 4, Supplementary Fig. S4).

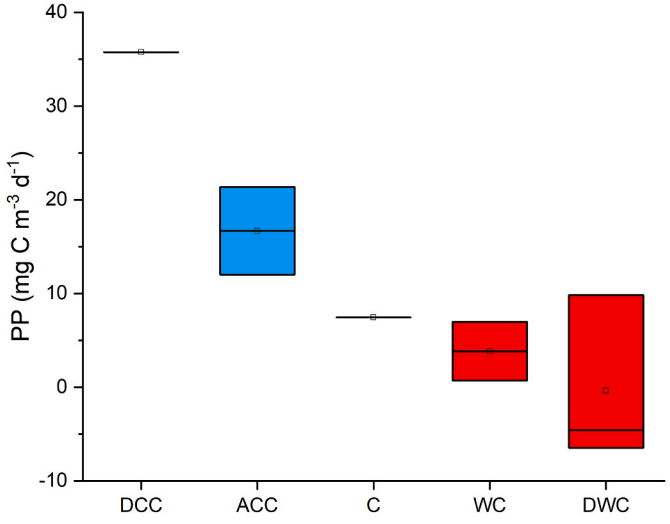

Fig. 4. Individual primary productivity (PP) values from all water masses sampled: dipole cold-core (DCC), aged cold-core (ACC), coastal (C), warm-core (WC), and dipole warm-core (DWC).

Table 3
Variance in phytoplankton community in all water masses explained by distance-based linear model (DistLM) analysis using physico-chemical variables consisting of the attenuation coefficient of surface irradiance, K_d (PAR), mixed layer depth (MLD), temperature, salinity and dissolved nutrients (NH_4^+, NO_x, PO_4^{3-} and Si). Shown are the most parsimonious solutions generated from all available variables (using the "best" model selection criteria), together with the Akaike information criterion statistic (AICc-the relative amount of information lost by a given model corrected for small sample number) and R-squared (percentage of variance explained by variable[s]) Significant P-values (<0.05) are indicated in bold text. Pseudo F = statistic for testing the general multivariate null hypothesis, Prop = the proportion of variability explained by the respective variable, and RSS = Residual Sum of Squares.

Marginal tests (n = 10)	Pseudo-F	P	Prop.
Temperature	451.7	8.258	0.035
Salinity	16.21	**0.006**	0.698
K_d (PAR)	10.03	**0.002**	0.589
Si	3.16	0.083	0.311
NH_4^+	0.79	0.365	0.101
MLD	75.40	0.695	0.498
Overall best solutions	**AICc**	**R^2**	**RSS**
K_d (PAR), Si	32.061	0.88553	95.54
Salinity	35.978	0.69844	251.68
Temperature, K_d (PAR), Si	36.392	0.91677	69.461

4. Discussion

Mesoscale eddies are key features of western boundary currents, yet their impact upon regional PP variability remains poorly understood. Our study provides new estimates of surface PP in mesoscale eddies in the East Australian Current System, with the largest number of eddies sampled concurrently to date. Although there have been several prior investigations of PP in the region, these have mainly involved satellite altimetry and ocean colour data (e.g. Condie and Dunn 2006; Chen et al., 2021) with only a handful of studies measuring PP in situ (Hassler et al., 2011; Everett and Doblin 2015; Doblin et al., 2016). Here, for the first time, we directly measure and compare PP across multiple eddy types in the EAC region during a single voyage, sampling an aged cold-core, a warm-core, and a dipole eddy pair in the western Tasman Sea.

Table 4
Variance in net primary productivity (PP), explained by distance-based linear modelling (DistLM) analysis using physico-chemical variables: attenuation coefficient of surface irradiance, K_d (PAR), mixed layer depth (MLD), temperature, salinity and nutrients (NH_4^+, and Si); biological variables: of size fractionated Chl *a*, pigments (Hex-19 fucoxanthin), pigment indices (Dia_{DP}, $Flag_{DP}$ and $Prok_{DP}$; photoprotective to photosynthetic pigments [PPC:PSC], Shannon-Wiener Diversity Index [H']); and a combination of both. Selected procedure was "best", with 9999 permutations. Specified solutions included only selected variables as listed. Shown are the most parsimonious solutions generated from all available variables, together with the Akaike information criterion statistic (AICc-the relative amount of information lost by a given model corrected for small sample number), percentage of variance explained by variable (R^2). Significant P-values (<0.05) are given in bold numbers. Pseudo F = statistic for testing the general multivariate null hypothesis, Prop = the proportion of variability explained by the respective variable.

Marginal tests (n = 9)	Pseudo-F	P	Prop.
Physico-chemical Variables			
Temperature	391.5	0.241	0.737
Salinity	0.886	0.226	0.112
Si	0.262	0.908	0.036
NH_4^+,	0.565	0.478	0.046
K_d(PAR)	2.904	0.104	0.293
MLD	1729	1.209	0.336
Biological Variables			
Chl *a* 2.0–10 μm	0.114	0.741	0.016
Chl *a* >10 μm	1.083	0.208	0.134
$Prok_{DP}$	6.065	**0.027**	0.464
$Flag_{DP}$	0.884	0.560	0.112
Dia_{DP}	0.600	0.418	0.078
19-Hex-Fucox	2478	1.873	0.130
PPC:PSC	4.651	**0.012**	0.399
H′	4.242	**0.022**	0.377

Overall Best Solutions	AICc	R^2
K_d (PAR), Temp, Si (*Physico-Chemical)*	76.89	0.467
Prok, H′, Chl >10 μm (*Biological*)	70.43	0.740
H', Temp, Si (*Physico-Chemical and Biological*)	71.57	0.704

Additional Models	AICc	R^2
K_d (PAR), Temp, Total Chl *a (remote sensed proxies)*	78.52	0.361
Size fractionated Chl *a*, Temp	83.18	0.717
Size fractionated Chl *a*,Temp, K_d (PAR)	105.17	0.774

4.1. Spatial variation in PP and comparison of eddy types

We found that PP differed between eddies in this region, ranging from as low as 0 mg C m^{-3} d^{-1} in an EAC-derived warm-core eddy, to as high as ~35 mg C m^{-3} d^{-1} in a recently-formed (dipole) cold-core eddy. The coastal reference station exhibited intermediate PP, indicating that eddies may exhibit greater or lower rates of primary productivity compared to adjacent water masses.

Although PP in the aged cold-core eddy was depressed relative to the newly-formed dipole cold-core eddy, it was still significantly higher than in either of the warm-core eddies sampled (Fig. 4). Satellite based estimates of PP in the aged cold core had greatest divergence with our measurements (relatively low compared to the ^{13}C values), indicating that the prevailing physico-chemical and Chl *a* signatures alone are likely not enough for algorithms to reliably predict PP within a cold-core eddy. Because eddy source water, size and eddy life-stage/age all influence phytoplankton species composition and overall PP (Chen et al., 2021; Eden and Dietze, 2009), a dipole eddy pair (i.e., eddies of the same age, size and phase, but contrasting physico-chemical environments) represents an ideal system to examine biotic and abiotic factors regulating PP in the absence of confounding temporal effects.

In the dipole eddy pair that we examined, the cold-core eddy was found to be 35-fold more productive than its warm counterpart, presumably driven by the dominance of large diatoms, as evidenced by HPLC analysis and Chl *a* size fractionation (Fig. 3a and b). Previous studies of cold-core eddies off Hawaii (Vaillancourt et al., 2003), northwest Atlantic (McGillicuddy et al., 2007), northwest Pacific (Kwak et al., 2014), the Red Sea (Kheireddine et al., 2017) and eastern Australia (Doblin et al., 2016) have similarly shown that large diatoms are the most prominent taxa and contributor to PP in surface waters, compared to picophytoplankton found in less-productive, surrounding oligotrophic waters. The increased productivity in the dipole cold-core eddy in our study was likely a result of isopycnal uplift of high nutrient and cold continental slope water into the euphotic zone (e.g., Hallegraeff and Jeffrey 1993) promoting diatom bloom formation, in contrast to the dipole warm-core eddy, that was dominated by smaller haptophytes and pelagophytes. Previous studies of phytoplankton composition in the EAC region routinely show a prevalence of picocyanobacteria, such as *Prochlorococcus* and *Synechococcus*, except for occasional diatom blooms associated with periodic instabilities in the water column that favour high NO_x and Si concentrations, such as cold-core eddies or frontal boundaries (Doblin et al., 2016; Thompson et al., 2011). Nanophytoplankton dominated the phytoplankton community observed in a warm-core eddy (Jeffrey and Hallegraeff, 1980), where pennate diatoms were the most prevalent taxa, followed by coccolithophorids and green flagellates, with minimal compositional differences to surrounding waters. Our relatively limited observations in this study suggest pennate diatoms may be more prominent in downwelling warm-core eddies, while conversely centric diatoms are more prominent in cold-core eddies - even when in apparent decay, such as in the aged cold-core eddy (Table 2). Just as a large surface area-to-volume ratio offers small-sized phytoplankton a competitive advantage under low nutrient concentrations, (Cotner and Biddanda, 2002; Thingstad & Sakshaug, 1990), it is likely that pennate diatoms possess traits that confer a competitive advantage in oligotrophic environments, such as inherently lower nutrient requirements, capacity to employ dormancy, and increased resistance to grazing (Ardyna and Arrigo, 2020; Petrucciani et al., 2022; Pilkaityte and Razinkovas, 2007).

Our measured values for PP fall within the range of previous observations from mesoscale eddies in this region, which range from ~1.4–57 mg C m^{-3} d^{-1} in the spring (Hassler et al., 2011; Everett and Doblin 2015), and 3.5–13.5 mg C m^{-3} d^{-1} during the less-productive autumn season (Chen et al., 2021). Our observation that PP was significantly enhanced in the dipole cold-core eddy compared to nearby water masses (i.e., the dipole warm-core counterpart) is consistent with findings of Hassler et al. (2011) who reported PP rates 13-fold higher in an oceanic cold-core eddy compared to surrounding EAC waters. While comparing PP values across studies can be problematic due to inherent differences in methodology (see Regaudie-de-Gioux et al., 2014; Hughes et al., 2018a), compiling PP values from other regions, reveals a consistent pattern of large intra-regional variability in PP associated with the presence of mesoscale eddies (Supplementary Table S3). Indeed, our study adds to an expanding body of research confirming mesoscale eddies exert significant influence over PP compared to surrounding water masses, presumably driven by the dynamic light, temperature and nutrient environments experienced by phytoplankton assemblages in such areas (Baltar et al., 2010; Roughan et al., 2011; Thompson et al., 2011).

4.2. Temporal variation in PP

While this study focussed on spatial variation in PP, we were able to re-sample the aged cold-core eddy on successive days (Supplementary Table S1). NO_x levels were the lowest of all stations sampled, while NH_4^+, levels showed a marginal increase over 24 h, perhaps indicating recycling of nitrogen by phytoplankton. Furthermore, Chl *a* declined 50% over the same period (from 0.56 to 0.25 μg L^{-1}; Supplementary Table S1) and corresponded to a decline in PP. Such findings appear consistent with those of a previous temporal study of a cold-core eddy in the Kuroshio current where the concentration of inorganic nitrogen was almost entirely depleted after five days; Chl *a* declined due to nutrients being exhausted, as well as grazing and sinking processes, leading to

declining PP rates (Kimura et al., 1997). It is worth noting however, that because we sampled across only two points, it is possible that the patterns observed could be driven by spatial rather than temporal variability. By the end of September, the aged cold-core eddy in our study had largely dissipated, with surface water temperatures inside the residual eddy similar to that of the surrounding water – whether PP had receded to background levels in the Tasman Sea remains unclear.

4.3. Predicting primary productivity

Our statistical modelling revealed that the physico-chemical parameters that were associated with changes in phytoplankton composition (i.e., K_d, Si, salinity) mapped to 47% of the variation in PP. However, when biological variables were also included, more than 70% of the variation in PP between water masses was explained. The biological parameters that were significant included aspects of phytoplankton composition (prokaryotes, diversity H') as well as photophysiology (PPC:PSC). However, the inclusion of size-fractionated Chl *a* caused an equivalent increase in model predictive power as the other biological parameters, while being considerably more cost-effective to measure. We conclude that mesoscale eddies alter primary production through altering phytoplankton community composition, and that information about the community size structure could therefore improve estimates of PP in our study region.

Notwithstanding the relatively small sample size in this study, our model analysis selected prokaryotes (specifically the picocyanobacteria *Prochlorococcus* and *Synechococcus*), K_d (PAR) and the Shannon-Weiner Diversity Index as most powerful predictors of PP. Small-sized prokaryote phytoplankton are often identified as "gleaners," adapted to low nutrient, oligotrophic environments (Barton et al., 2010) such as the EAC and the warm-core eddies sampled in this study (Armbrecht et al., 2014; Hallegraeff and Jeffrey, 1993), but fix relatively less carbon per cell than larger celled eukaryotes. In warm-core eddies, K_d (PAR) is greater as light penetrates further into the deep mixed layer, and phytoplankton must synthesise photoprotective pigments to prevent photoinhibition (i.e. increase their PPC:PSC), and in doing so, often sacrifice photosynthetic efficiency (Berner et al., 1989). Inclusion of a biodiversity metric (i.e., Shannon-Weiner diversity index calculated from pigment data) also improved our ability to model PP variability but the non-linear relationship between diversity and primary productivity (Fraser et al., 2015; Vallina et al., 2014), as well as the relatively low number of samples in this study suggest that this result should be treated with caution.

For modelers using satellite-derived models to predict PP (Friedrichs et al., 2009; Laiolo et al., 2016; Lee et al., 2015; Rocha et al., 2019), there are typically limited in situ measurements. We therefore attempted to model eddy PP using common input fields in such models (i.e., sea surface temperature, K_d [PAR], Total Chl *a*), which resulted in only 36% of PP variability being explained by our statistical model. Importantly, including size fractionated Chl *a* as a predictor variable generated a significant improvement to model performance – indicating that even the simplest taxonomic information could clearly be beneficial for efforts to understand eddy-driven intra-regional PP variability. However, an important consideration is that chlorophyll-based satellite models often underestimate chlorophyll content due to pigment packaging effects (Laiolo et al., 2021). To reduce the uncertainty in satellite-based PP estimates, a fruitful area of research would be the collection of in situ data linking phytoplankton size structure to bio-optical properties.

The source water of an eddy likely wields considerable influence over the successional trajectories of phytoplankton assemblages relative to adjacent waters. Consequently, the eddy origin is a key variable influencing initial phytoplankton composition, which ultimately influences PP. In our study although the warm-core and dipole warm-core eddies were both formed in early August, the WC phytoplankton community composition included *Prochlorococcus*, typical of oligotrophic waters, whereas the DWC did not. Armbrecht et al. (2014) compared conditions of upwelling and downwelling events off Eastern Australia (~30°S) and determined that phytoplankton composition was dependent on whether the EAC was strong enough to promote upwelling deep into the continental shelf to uplift not only nutrients, but entrain cosmopolitan species, such as diatoms (typically associated with high productivity). Conversely, when the EAC did not reach the continental shelf, the phytoplankton composition was instead dominated by warm water, tropical phytoplankton species (Armbrecht et al., 2014). This suggests that an eddy formed at the EAC front could potentially entrain a range of phytoplankton communities, depending on how close the EAC was to the continental shelf.

Importantly, the physico-chemical environment within an eddy is not instantaneously correlated with the biology – rather the trajectory of phytoplankton succession and biogeochemical activity is a product of accumulated effects of advective processes, nutrient supply, irradiance, and key biological processes such as grazing (Fu et al., 2016). Although the environment and nutrient profile initially selects for phytoplankton taxa with particular traits, the lag-time between the uptake of nutrients, the growth rate of phytoplankton, the ensuing bloom, and the subsequent availability of nutrients, may alter the compositional structure, with a cascading impact on PP. Therefore, eddy-driven PP variability is ultimately regulated by numerous physico-chemical and biological factors that vary in space and time. Interestingly, in our study, the aged cold-core eddy (three months old) exhibited characteristics of both cold- and warm-core eddies. While the negative sea-level anomaly, shallow nutricline, cooler temperature relative to surrounding waters, and clockwise geostrophic current were all consistent with characteristics of cold-core eddies (McGillicuddy, 2016), other chemical and biological characteristics more closely resembled those of oligotrophic waters. Specifically, low surface Chl *a* and low dissolved NO_x^- coupled with high NH_4^+, are usually associated with warm-core eddies and provide clear evidence of age-induced decay and associated recycling of nitrogen by phytoplankton (D'Alelio et al., 2020).

5. Conclusions

Our study found that surface PP in eastern Australian eddies is variable and can range from 0 to 35 mg C m^{-3} d^{-1} depending on the type of eddy, its life-stage and phytoplankton community composition, impacting local PP rates. Prediction of primary production is substantially improved by information on phytoplankton size structure, according to our statistical model. In situ sampling, although costly and time-consuming, continues to yield important data, and is essential for validation of satellite-derived products. Encouragingly, the imminent Plankton, Aerosol, Cloud, ocean Ecosystem (PACE) mission from NASA, includes a new sensor with continuous 5 nm spectral resolution from the UV to the near infrared, designed to provide more information that could help resolve the phytoplankton community composition and potentially improve primary productivity estimates from space (http://pace.oceansciences.org). To further address uncertainties in PP estimates, future studies would benefit from investigating the temporal evolution of cold-core eddies including phytoplankton traits and species composition, and the associated depth-related effect on PP, to provide a more complete picture of their contribution to global PP and the carbon cycle.

Declaration of competing interest

The authors declare that they have no known competing financial interests or personal relationships that could have appeared to influence the work reported in this paper.

Data availability

Data will be made available on request.

Acknowledgments

This research was supported by the Marine National Facility RV Investigator and the Australian Research Council's Discovery Projects scheme DP140101340 and DP180100054 to MD. We thank the captain, crew and scientific support team of the *RV Investigator* who helped facilitate our sample collection. G.F.F. is supported by an Australian Government Training Program Scholarship.

Appendix A. Supplementary data

Supplementary data to this article can be found online at https://doi.org/10.1016/j.dsr.2022.103952.

References

Anderson, M.J., Gorley, R.N., Clarke, K.R., 2008. PERMANOVA+ for PRIMER: guide to software and statistical methods. In Plymouth, UK (pp. 1–214). https://www.researchgate.net/publication/285237419_PERMANOVA_for_primer_Guide_to_software_and_statistical_methods.

Arar, E.J., Collins, G.B., 1997. Method 445.0 in vitro determination of chlorophyll a and pheophytin a in marine and freshwater phytoplankton by fluorescence. In: Methods for the Determination of Chemical Substances in Marine and Estuarine Environmental Matrices, 445.01–445.22.

Archer, M., Schaeffer, A., Keating, S., Roughan, M., Holmes, R., Siegelman, L., 2020. Observations of submesoscale variability and frontal subduction within the mesoscale eddy field of the Tasman Sea. J. Phys. Oceanogr. 50 (5), 1509–1529. https://doi.org/10.1175/JPO-D-19-0131.1.

Ardyna, M., Arrigo, K.R., 2020. Phytoplankton dynamics in a changing arctic ocean. Nat. Clim. Change 10 (10), 892–903. https://doi.org/10.1038/s41558-020-0905-y.

Armbrecht, L.H., Roughan, M., Rossi, V., Schaeffer, A., Davies, P.L., Waite, A.M., Armand, L.K., 2014. Phytoplankton composition under contrasting oceanographic conditions: upwelling and downwelling (Eastern Australia). Continent. Shelf Res. 75, 54–67. https://doi.org/10.1016/j.csr.2013.11.024.

Baird, M.E., Suthers, I.M., Griffin, D.A., Hollings, B., Pattiaratchi, C., Everett, J.D., Roughan, M., Oubelkheir, K., Doblin, M., 2011. The effect of surface flooding on the physical-biogeochemical dynamics of a warm-core eddy off southeast Australia. Deep-Sea Res. Part II Top. Stud. Oceanogr. 58 (5), 592–605. https://doi.org/10.1016/j.dsr2.2010.10.002.

Baltar, F., Arístegui, J., Gasol, J.M., Lekunberri, I., Herndl, G.J., 2010. Mesoscale eddies: hotspots of prokaryotic activity and differential community structure in the ocean. ISME J. 4 (8), 975–988. https://doi.org/10.1038/ismej.2010.33.

Barlow, R., Stuart, V., Lutz, V., Sessions, H., Sathyendranath, S., Platt, T., Kyewalyanga, M., Clementson, L., Fukasawa, M., Watanabe, S., Devred, E., 2007. Seasonal pigment patterns of surface phytoplankton in the subtropical southern hemisphere. Deep-Sea Res. Part I Oceanogr. Res. Pap. 54 (10), 1687–1703. https://doi.org/10.1016/j.dsr.2007.06.010.

Barton, A.D., Dutkiewicz, S., Flierl, G., Bragg, J., Follows, M.J., 2010. Patterns of diversity in marine phytoplankton. Science 327 (5972), 1509–1511. https://doi.org/10.1126/science.1184961.

Behrenfeld, M.J., Falkowski, P.G., 1997. Photosynthetic rates derived from satellite-based chlorophyll concentration. Limnol. Oceanogr. 42 (1), 1–20. https://doi.org/10.4319/lo.1997.42.1.0001.

Berner, T., Dubinsky, Z., Wyman, K., Falkowski, P.G., 1989. Photoadaptation and the "package" effect in dunaliella tertiolecta (chlorophyceae). J. Phycol. 25 (1), 70–78. https://doi.org/10.1111/j.0022-3646.1989.00070.x.

Cetina-Heredia, P., Roughan, M., Van Sebille, E., Coleman, M.A., 2014. Long-term trends in the East Australian Current separation latitude and eddy driven transport. J. Geophys. Res.: Oceans 119 (7), 4351–4366. https://doi.org/10.1002/2014JC010071.

Cetina-Heredia, P., Roughan, M., van Sebille, E., Keating, S., Brassington, G.B., 2019. Retention and leakage of water by mesoscale eddies in the East Australian current system. J. Geophys. Res.: Oceans 124 (4), 2485–2500. https://doi.org/10.1029/2018JC014482.

Chelton, D.B., Schlax, M.G., Samelson, R.M., 2011. Global observations of nonlinear mesoscale eddies. Prog. Oceanogr. 91 (2), 167–216. https://doi.org/10.1016/j.pocean.2011.01.002.

Chen, X., Schallenberg, C., Phillips, H., Chase, Z., 2021. Biogeochemical characteristics of eddies in the East Australian Current depend on eddy type, history and location. J. Mar. Syst. 216, 103512 https://doi.org/10.1016/j.jmarsys.2021.103512.

Claustre, H., Kerherve, P., Marty, J.C., Prieur, L., Videau, C., Hecq, J.H., 1994. Phytoplankton dynamics associated with a geostrophic front: ecological and biogeochemical implications. J. Mar. Res. 52 (4), 711–742. https://doi.org/10.1357/0022240943077000.

Condie, S.A., Dunn, J.R., 2006. Seasonal characteristics of the surface mixed layer in the Australasian region: implications for primary production regimes and biogeography. Mar. Freshw. Res. 57 (6), 569–590. https://doi.org/10.1071/MF06009.

Cotner, J.B., Biddanda, B.A., 2002. Small players, large role: microbial influence on biogeochemical processes in pelagic aquatic ecosystems. Ecosystems 5 (2), 105–121. https://doi.org/10.1007/s10021-001-0059-3.

D'Alelio, D., Rampone, S., Cusano, L.M., Morfino, V., Russo, L., Sanseverino, N., Cloern, J.E., Lomas, M.W., 2020. Machine learning identifies a strong association between warming and reduced primary productivity in an oligotrophic ocean gyre. Sci. Rep. 10 (1), 1–12. https://doi.org/10.1038/s41598-020-59989-y.

Doblin, M.A., Petrou, K., Sinutok, S., Seymour, J.R., Messer, L.F., Brown, M.V., Norman, L., Everett, J.D., McInnes, A.S., Ralph, P.J., Thompson, P.A., Hassler, C.S., 2016. Nutrient uplift in a cyclonic eddy increases diversity, primary productivity and iron demand of microbial communities relative to a western boundary current. PeerJ 2016 (4), e1973. https://doi.org/10.7717/peerj.1973.

Dufois, F., Hardman-Mountford, N.J., Fernandes, M., Wojtasiewicz, B., Shenoy, D., Slawinski, D., Gauns, M., Greenwood, J., Toresen, R., 2017. Observational insights into chlorophyll distributions of subtropical South Indian Ocean eddies. Geophys. Res. Lett. 44 (7), 3255–3264. https://doi.org/10.1002/2016GL072371.

Dutkiewicz, S., Hickman, A.E., Jahn, O., Henson, S., Beaulieu, C., Monier, E., 2019. Ocean colour signature of climate change. Nat. Commun. 10 (1), 1–13. https://doi.org/10.1038/s41467-019-08457-x.

Eden, C., Dietze, H., 2009. Effects of mesoscale eddy/wind interactions on biological new production and eddy kinetic energy. J. Geophys. Res.: Oceans 114 (5), 5023. https://doi.org/10.1029/2008JC005129.

Everett, J.D., Baird, M.E., Oke, P.R., Suthers, I.M., 2012. An avenue of eddies: quantifying the biophysical properties of mesoscale eddies in the Tasman Sea. Geophys. Res. Lett. 39 (16), 16608 https://doi.org/10.1029/2012GL053091.

Everett, J.D., Doblin, M.A., 2015. Characterising primary productivity measurements across a dynamic western boundary current region. Deep-Sea Res. Part I Oceanogr. Res. Pap. 100, 105–116. https://doi.org/10.1016/j.dsr.2015.02.010.

Falkowski, P.G., Ziemann, D., Kolber, Z., Bienfang, P.K., 1991. Role of eddy pumping in enhancing primary production in the ocean. Nature 352 (6330), 55–58. https://doi.org/10.1038/352055a0.

Fraser, L.H., Pither, J., Jentsch, A., Sternberg, M., Zobel, M., Askarizadeh, D., Bartha, S., Beierkuhnlein, C., Bennett, J.A., Bittel, A., Boldgiv, B., Boldrini, I.I., Bork, E., Brown, L., Cabido, M., Cahill, J., Carlyle, C.N., Campetella, G., Chelli, S., et al., 2015. Worldwide evidence of a unimodal relationship between productivity and plant species richness. Science 349 (6245), 302–305. https://doi.org/10.1126/science.aab3916.

Friedrichs, M.A.M., Carr, M.E., Barber, R.T., Scardi, M., Antoine, D., Armstrong, R.A., Asanuma, I., Behrenfeld, M.J., Buitenhuis, E.T., Chai, F., Christian, J.R., Ciotti, A.M., Doney, S.C., Dowell, M., Dunne, J., Gentili, B., Gregg, W., Hoepffner, N., Ishizaka, J., et al., 2009. Assessing the uncertainties of model estimates of primary productivity in the tropical Pacific Ocean. J. Mar. Syst. 76 (1–2), 113–133. https://doi.org/10.1016/j.jmarsys.2008.05.010.

Fu, W., Randerson, J.T., Keith Moore, J., 2016. Climate change impacts on net primary production (NPP) and export production (EP) regulated by increasing stratification and phytoplankton community structure in the CMIP5 models. Biogeosciences 13 (18), 5151–5170. https://doi.org/10.5194/bg-13-5151-2016.

Hallegraeff, G.M., Jeffrey, S.W., 1993. Annually recurrent diatom blooms in spring along the new south wales coast of Australia. Mar. Freshw. Res. 44 (2), 325–334. https://doi.org/10.1071/MF9930325.

Hama, T., Miyazaki, T., Ogawa, Y., Iwakuma, T., Takahashi, M., Otsuki, A., Ichimura, S., 1983. Measurement of photosynthetic production of a marine phytoplankton population using a stable 13C isotope. Mar. Biol. 73 (1), 31–36. https://doi.org/10.1007/BF00396282.

Hassler, C.S., Djajadikarta, J.R., Doblin, M.A., Everett, J.D., Thompson, P.A., 2011. Characterisation of water masses and phytoplankton nutrient limitation in the East Australian Current separation zone during spring 2008. Deep-Sea Res. Part II Top. Stud. Oceanogr. 58 (5), 664–677. https://doi.org/10.1016/j.dsr2.2010.06.008.

Hughes, D.J., Campbell, D.A., Doblin, M.A., Kromkamp, J.C., Lawrenz, E., Moore, C.M., Oxborough, K., Prášil, O., Ralph, P.J., Alvarez, M.F., Suggett, D.J., 2018a. Roadmaps and detours: active chlorophyll- a assessments of primary productivity across marine and freshwater systems. In: Environmental Science and Technology, vol. 52. American Chemical Society, pp. 12039–12054. https://doi.org/10.1021/acs.est.8b03488. Issue 21.

Hughes, D.J., Crosswell, J.R., Doblin, M.A., Oxborough, K., Ralph, P.J., Varkey, D., Suggett, D.J., 2020. Dynamic variability of the phytoplankton electron requirement for carbon fixation in eastern Australian waters. J. Mar. Syst. 202, 103252 https://doi.org/10.1016/j.jmarsys.2019.103252.

Hughes, D.J., Varkey, D., Doblin, M.A., Ingleton, T., Mcinnes, A., Ralph, P.J., van Dongen-Vogels, V., Suggett, D.J., 2018b. Impact of nitrogen availability upon the electron requirement for carbon fixation in Australian coastal phytoplankton communities. Limnol. Oceanogr. 63 (5), 1891–1910. https://doi.org/10.1002/lno.10814.

Jeffrey, S., Hallegraeff, G., 1980. Studies of phytoplankton species and photosynthetic pigments in a warm core eddy of the East Australian current. I. Summer populations. Mar. Ecol. Prog. Ser. 3, 285–294. https://doi.org/10.3354/meps003285.

Kamenkovich, V.M., Koshlyakov, M.N., Monin, A.S., 1986. Eddies of western boundary currents. Synoptic Eddies Ocean 208–264. https://doi.org/10.1007/978-94-009-4502-9_4.

Kara, A.B., Rochford, P.A., Hurlburt, H.E., 2000. An optimal definition for ocean mixed layer depth. J. Geophys. Res.: Oceans 105 (C7), 16803–16821. https://doi.org/10.1029/2000jc900072.

Kheireddine, M., Ouhssain, M., Claustre, H., Uitz, J., Gentili, B., Jones, B.H., 2017. Assessing pigment-based phytoplankton community distributions in the Red Sea. Front. Mar. Sci. 4 (MAY), 132. https://doi.org/10.3389/fmars.2017.00132.

Kimura, S., Kasai, A., Nakata, H., Sugimoto, T., Simpson, J.H., Cheok, J.V.S., 1997. Biological productivity of meso-scale eddies caused by frontal disturbances in the Kuroshio. ICES (Int. Counc. Explor. Sea) J. Mar. Sci. 54 (2), 179–192. https://doi.org/10.1006/jmsc.1996.0209.

Kwak, J.H., Lee, S.H., Hwang, J., Suh, Y.S., Je Park, H., Chang, K. Il, Kim, K.R., Kang, C. K., 2014. Summer primary productivity and phytoplankton community composition driven by different hydrographic structures in the East/Japan Sea and the Western Subarctic Pacific. J. Geophys. Res.: Oceans 119 (7), 4505–4519. https://doi.org/10.1002/2014JC009874.

Kwong, L.E., Henschke, N., Pakhomov, E.A., Everett, J.D., Suthers, I.M., 2020. Mesozooplankton and micronekton active carbon transport in contrasting eddies. Front. Mar. Sci. 6, 825. https://doi.org/10.3389/fmars.2019.00825.

Laiolo, L., Matear, R., Baird, M.E., Soja-Woźniak, M., Doblin, M.A., 2018. Information content of in situ and remotely sensed chlorophyll-a: learning from size-structured phytoplankton model. J. Mar. Syst. 183, 1–12. https://doi.org/10.1016/j.jmarsys.2018.03.005.

Laiolo, L., Matear, R., Soja-Woźniak, M., Suggett, D.J., Hughes, D.J., Baird, M.E., Doblin, M.A., 2021. Modelling the impact of phytoplankton cell size and abundance on inherent optical properties (IOPs) and a remotely sensed chlorophyll-a product. J. Mar. Syst. 213, 103460 https://doi.org/10.1016/j.jmarsys.2020.103460.

Laiolo, L., McInnes, A.S., Matear, R., Doblin, M.A., 2016. Key drivers of seasonal plankton dynamics in cyclonic and anticyclonic eddies off East Australia. Front. Mar. Sci. 3 (AUG), 155. https://doi.org/10.3389/fmars.2016.00155.

Lee, Y.J., Matrai, P.A., Friedrichs, M.A.M., Saba, V.S., Antoine, D., Ardyna, M., Asanuma, I., Babin, M., Bélanger, S., Benoît-Gagné, M., Devred, E., Fernández-Méndez, M., Gentili, B., Hirawake, T., Kang, S.H., Kameda, T., Katlein, C., Lee, S.H., Lee, Z., et al., 2015. An assessment of phytoplankton primary productivity in the Arctic Ocean from satellite ocean color/in situ chlorophyll-a based models. J. Geophys. Res.: Oceans 120 (9), 6508–6541. https://doi.org/10.1002/2015JC011018.

Mahadevan, A., 2016. The impact of submesoscale physics on primary productivity of plankton. Ann. Rev. Mar. Sci 8, 161–184. https://doi.org/10.1146/annurev-marine-010814-015912.

Mahadevan, A., Campbell, J.W., 2002. Biogeochemical patchiness at the sea surface. Geophys. Res. Lett. 29 (19) https://doi.org/10.1029/2001GL014116, 32–1.

Malan, N., Archer, M., Roughan, M., Cetina-Heredia, P., Hemming, M., Rocha, C., Schaeffer, A., Suthers, I., Queiroz, E., 2020. Eddy-driven cross-shelf transport in the East Australian current separation zone. J. Geophys. Res.: Oceans 125 (2), e2019JC015613. https://doi.org/10.1029/2019JC015613.

Martin, A.P., Richards, K.J., Bracco, A., Provenzale, A., 2002. Patchy productivity in the open ocean. Global Biogeochem. Cycles 16 (2). https://doi.org/10.1029/2001gb001449, 9-1-9–9.

Matear, R.J., Chamberlain, M.A., Sun, C., Feng, M., 2013. Climate change projection of the Tasman Sea from an eddy-resolving ocean model. J. Geophys. Res.: Oceans 118 (6), 2961–2976. https://doi.org/10.1002/jgrc.20202.

McGillicuddy, D.J., 2016. Mechanisms of physical-biological-biogeochemical interaction at the oceanic mesoscale. Ann. Rev. Mar. Sci 8, 125–159. https://doi.org/10.1146/annurev-marine-010814-015606.

McGillicuddy, D.J., Anderson, L.A., Bates, N.R., Bibby, T., Buesseler, K.O., Carlson, C.A., Davis, C.S., Ewart, C., Falkowski, P.G., Goldthwait, S.A., Hansell, D.A., Jenkins, W.J., Johnson, R., Kosnyrev, V.K., Ledwell, J.R., Li, Q.P., Siegel, D.A., Steinberg, D.K., 2007. Eddy/Wind interactions stimulate extraordinary mid-ocean plankton blooms. Science 316 (5827), 1021–1026. https://doi.org/10.1126/science.1136256.

McIlgorm, A., Hanna, S., Knapp, G., Le Floc'H, P., Millerd, F., Pan, M., 2010. How will climate change alter fishery governance{glottal stop} Insights from seven international case studies. Mar. Pol. 34 (1), 170–177. https://doi.org/10.1016/j.marpol.2009.06.004.

Milutinović, S., Bertino, L., 2011. Assessment and propagation of uncertainties in input terms through an ocean-color-based model of primary productivity. Rem. Sens. Environ. 115 (8), 1906–1917. https://doi.org/10.1016/j.rse.2011.03.013.

Morris, D.P., 2009. Optical properties of water. In: Encyclopedia of Inland Waters. Elsevier Inc, pp. 682–689. https://doi.org/10.1016/B978-012370626-3.00069-7.

Noble, P.A., Tymowski, R.G., Fletcher, M., Morris, J.T., Lewitus, A.J., 2003. Contrasting patterns of phytoplankton community pigment composition in two salt marsh estuaries in southeastern United States. Appl. Environ. Microbiol. 69 (7), 4129–4143. https://doi.org/10.1128/AEM.69.7.4129-4143.2003.

Oke, P.R., Griffin, D.A., 2011. The cold-core eddy and strong upwelling off the coast of New South Wales in early 2007. Deep-Sea Res. Part II Top. Stud. Oceanogr. 58 (5), 574–591. https://doi.org/10.1016/j.dsr2.2010.06.006.

Oke, P.R., Roughan, M., Cetina-Heredia, P., Pilo, G.S., Ridgway, K.R., Rykova, T., Archer, M.R., Coleman, R.C., Kerry, C.G., Rocha, C., Schaeffer, A., Vitarelli, E., 2019. Revisiting the circulation of the East Australian Current: its path, separation, and eddy field. In: Progress in Oceanography, vol. 176. Elsevier Ltd, 102139. https://doi.org/10.1016/j.pocean.2019.102139.

Petrucciani, A., Chaerle, P., Norici, A., 2022. Diatoms versus copepods: could frustule traits have a role in avoiding predation? Front. Mar. Sci. 8 (February), 1–13. https://doi.org/10.3389/fmars.2021.804960.

Pilkaityte, R., Razinkovas, A., 2007. Seasonal changes in phytoplankton composition and nutrient limitation in a shallow Baltic lagoon. Boreal Environ. Res. 12 (5), 551–559.

Rees, C., Pender, L., Sherrin, K., Schwanger, C., Hughes, P., Tibben, S., Marouchos, A., Rayner, M., 2019. Methods for reproducible shipboard SFA nutrient measurement using RMNS and automated data processing. Limnol Oceanogr. Methods 17 (1), 25–41. https://doi.org/10.1002/lom3.10294.

Regaudie-de-Gioux, A., Lasternas, S., Agustí, S., Duarte, C.M., 2014. Comparing marine primary production estimates through different methods and development of conversion equations. In: Frontiers in Marine Science, vol. 1. Frontiers Media S. A, p. 19. https://doi.org/10.3389/fmars.2014.00019. Issue JUL.

Ridgway, K.R., 1997. Seasonal cycle of the East Australian current. J. Geophys. Res. C Oceans 102 (C10), 22921–22936. https://doi.org/10.1029/97JC00227.

Rocha, C., Edwards, C.A., Roughan, M., Cetina-Heredia, P., Kerry, C., 2019. A high-resolution biogeochemical model (ROMS 3.4+bio-Fennel) of the East Australian current system. Geosci. Model Dev. (GMD) 12 (1), 441–456. https://doi.org/10.5194/gmd-12-441-2019.

Roughan, M., Keating, S.R., Schaeffer, A., Cetina Heredia, P., Rocha, C., Griffin, D., Robertson, R., Suthers, I.M., 2017. A tale of two eddies: the biophysical characteristics of two contrasting cyclonic eddies in the East Australian Current System. J. Geophys. Res.: Oceans 122 (3), 2494–2518. https://doi.org/10.1002/2016JC012241.

Roughan, M., Macdonald, H.S., Baird, M.E., Glasby, T.M., 2011. Modelling coastal connectivity in a western boundary current: seasonal and inter-annual variability. Deep-Sea Res. Part II Top. Stud. Oceanogr. 58 (5), 628–644. https://doi.org/10.1016/j.dsr2.2010.06.004.

Schaeffer, A., Gramoulle, A., Roughan, M., Mantovanelli, A., 2017. Characterizing frontal eddies along the East Australian Current from HF radar observations. J. Geophys. Res.: Oceans 122 (5), 3964–3980. https://doi.org/10.1002/2016JC012171.

Strickland, J.D.H., Parsons, T.R., 1972. DFO-A practical handbook of seawater analysys. In: Fisheries Research Board of Canada, second ed. https://doi.org/10.1086/406210

Suthers, I.M., Young, J.W., Baird, M.E., Roughan, M., Everett, J.D., Brassington, G.B., Byrne, M., Condie, S.A., Hartog, J.R., Hassler, C.S., Hobday, A.J., Holbrook, N.J., Malcolm, H.A., Oke, P.R., Thompson, P.A., Ridgway, K., 2011. The strengthening East Australian Current, its eddies and biological effects - an introduction and overview. In: Deep-Sea Research Part II: Topical Studies in Oceanography, vol. 58. Pergamon, pp. 538–546. https://doi.org/10.1016/j.dsr2.2010.09.029. Issue 5.

Thingstad, T., Sakshaug, E., 1990. Control of phytoplankton growth in nutrient recycling ecosystems. Theory and terminology. Mar. Ecol. Prog. Ser. 63, 261–272. https://doi.org/10.3354/meps063261.

Thompson, P.A., Bonham, P., Waite, A.M., Clementson, L.A., Cherukuru, N., Hassler, C., Doblin, M.A., 2011. Contrasting oceanographic conditions and phytoplankton communities on the east and west coasts of Australia. Deep-Sea Res. Part II Top. Stud. Oceanogr. 58 (5), 645–663. https://doi.org/10.1016/j.dsr2.2010.10.003.

Vaillancourt, R.D., Marra, J., Seki, M.P., Parsons, M.L., Bidigare, R.R., 2003. Impact of a cyclonic eddy on phytoplankton community structure and photosynthetic competency in the subtropical North Pacific Ocean. Deep-Sea Res. Part I Oceanogr. Res. Pap. 50 (7), 829–847. https://doi.org/10.1016/S0967-0637(03)00059-1.

Vallina, S.M., Follows, M.J., Dutkiewicz, S., Montoya, J.M., Cermeno, P., Loreau, M., 2014. Global relationship between phytoplankton diversity and productivity in the ocean. Nat. Commun. 5 https://doi.org/10.1038/ncomms5299.

Westberry, T., Behrenfeld, M.J., Siegel, D.A., Boss, E., 2008. Carbon-based primary productivity modeling with vertically resolved photoacclimation. Global Biogeochem. Cycles 22 (2). https://doi.org/10.1029/2007GB003078.